



Precipitation kinetics and morphology evolution of the $\text{Co}_3(\text{Al}, \text{W})$ phase in a medium supersaturation Co–Al–W alloy

Shujing Shi^{1,2}, Zhengwei Yan^{1,2}, Yongsheng Li^{1,2,*}, Dong Wang^{1,2}, Zhiheng An¹, Gang Sha¹, Yang Wang³, and Yan Zhao³

¹ School of Materials Science and Engineering, Nanjing University of Science and Technology, Nanjing 210094, China

² MIIT Key Laboratory of Advanced Metallic and Intermetallic Materials Technology, Nanjing 210094, China

³ School of Materials Science and Engineering, Shanghai University, Shanghai 200444, China

Received: 20 May 2020

Accepted: 13 September 2020

Published online:

12 October 2020

© Springer Science+Business Media, LLC, part of Springer Nature 2020

ABSTRACT

The effects of aging temperature on the precipitation of the γ' - $\text{Co}_3(\text{Al}, \text{W})$ phase were studied by utilizing transmission electron microscopy, scanning electron microscopy and atom probe tomography, with the aim of exploring the continuum kinetics of the γ' phase in the medium supersaturation Co–9Al–8W (at.%) alloy from early precipitation to later coarsening. The results showed that the γ' phases with small size and large number density caused a rapid increase in alloy microhardness at 1073 K when the aging time was less than 136 h, implying that precipitation strengthening clearly occurred. Due to the high thermodynamic driving force and small critical radius of nucleation, the γ' phases expeditiously precipitated within 0.08 h of aging. Additionally, the partitioning coefficients of the elements showed that the partitions of Al and W in the γ' phase were more obvious at 1073 K. The time exponents of the average particle radius were close to the value of 1/3 predicted by the Lifshitz–Slyozov–Wagner theory. The particle size distribution of the γ' phase was more consistent with the Brailsford–Wynblatt model in the early growth-dominated stage, whereas it matched well with the trans-interface diffusion-controlled model in the later concomitant growth and coarsening stages. This research revealed the intimate relationship among the morphology, mechanical properties and evolution kinetics of the γ' phase in a medium supersaturation Co–Al–W alloy.

Handling Editor: Sophie Primig.

Address correspondence to E-mail: ysli@njust.edu.cn

<https://doi.org/10.1007/s10853-020-05379-8>

Introduction

Cobalt-based superalloys have attracted substantial interest due to the discovery of $L1_2$ - $\text{Co}_3(\text{Al}, \text{W})$ precipitates in the γ -Co matrix [1, 2]. The γ' - $\text{Co}_3(\text{Al}, \text{W})$ phase has a similar lattice structure to the γ' - Ni_3Al phase in nickel-based superalloys, while the elements Al and W jointly occupy the corner position of the $L1_2$ structure. Previous studies have shown that the stabilization temperature of the γ' - $\text{Co}_3(\text{Al}, \text{W})$ phase [3, 4] is higher than that of other discovered A_3B -type γ' phases, such as Co_3Ta [5] and Co_3Ti [6], and the lower lattice mismatch of the geometrically close-packed $\text{Co}_3(\text{Al}, \text{W})$ phase is impactful for alloy strengthening [2]. In this γ' precipitated Co–Al–W alloy, a $\gamma + \gamma'$ two-phase region exists, wherein the Al content is in the range of 9.2–10 at.% and the W content in the range of 5.4–12 at.% at 1173 K. Owing to the stability of the $\gamma + \gamma'$ phase, the creep properties of the superalloy are highly enhanced [7, 8]. As a result of their excellent comprehensive performance, cobalt-based superalloys are currently regarded as promising candidates for high-temperature applications in turbine blades of aero-engines and industrial gas turbines [9–12].

For precipitation-strengthened alloys, the strengthening effect is determined by the size, quantity and spatial distribution of precipitates and the lattice mismatch between the matrix and the precipitates [13–16]. Hence, the morphology evolution and precipitation kinetics of the γ' phase in cobalt-based superalloys are extremely important for the mechanical properties of these materials. Therefore, research on the precipitation and coarsening of the γ' phase has been conducted in recent years. Souza et al. [17] showed that the precipitates in Co–8.8Al–7.3W (at.%) alloy are homogeneously distributed and display cuboidal morphology with their arrangement occurring along a $\langle 100 \rangle$ -type direction after 4 h of aging at 1173 K. After 256 h of aging at this temperature, a coagulation and coalescence mechanism occurred among some adjacent particles. Azzam et al. [18] explored the early-stage precipitation of the γ' phase in a low supersaturation Co–9.1Al–7W (at.%) alloy aged for 0.08–200 h at 1173 K. Although they were not able to observe the nucleation process in the experiment, they determined that the critical radius of the γ' phase was ~ 2.5 nm and that the driving force for nucleation was ~ 264

J mol^{-1} . Meher et al. [19] studied high supersaturation Co–10Al–10W (at.%) alloy aged for 256 h. They indicated that the time exponents of the average particle radius were 0.323 for 1073 K and 0.329 for 1173 K, and the coarsening rate constant increased from $0.07 \times 10^{-27} \text{ m}^3\text{s}^{-1}$ to $1.41 \times 10^{-27} \text{ m}^3\text{s}^{-1}$ due to the 100 K increase in aging temperature.

Several theories and models about the coarsening law have been adopted for precipitation kinetics [20–22]. The Lifshitz–Slyozov–Wagner (LSW) [23, 24] theory predicts the coarsening kinetics of the second phase and assumes that a zero volume fraction of spherical particles is dispersed in a supersaturated solid solution. As a matrix-diffusion-limited coarsening mechanism, the cube of the average particle radius and time follows the relationship of $\langle r \rangle^3 - \langle r_0 \rangle^3 = k_L t$, where $\langle r \rangle$ and $\langle r_0 \rangle$ are the average particle radius at aging time t and the beginning time of coarsening, respectively, and k_L is the rate constant. Additionally, the LSW theory assumes a scaling form of the particle size distribution (PSD). To show the influences of the volume fraction on particle coarsening, the Brailsford–Wynblatt (BW) [25] model was proposed, in which the possibility of coalescence of large particles is neglected as Ostwald ripening proceeds. The trans-interface diffusion-controlled (TIDC) [26] model was proposed to clarify the coarsening process on account of the diffusive transport through the coherent interface of ordered and disordered phases; it ignores the effect of the volume fraction on the kinetics and the scaled PSD. The TIDC model predicts a linear relationship between the square of the average particle radius and aging time by $\langle r \rangle^2 - \langle r_0 \rangle^2 = k_T t$, where k_T is the rate constant.

Previous studies on Co–Al–W alloys have mainly focused on high supersaturation alloys ($W > \sim 9$ at.%), such as Co–10Al–10W (at.%) alloys [19, 27], and low supersaturation alloys ($W \leq \sim 7$ at.%), such as Co–9.1Al–7W (at.%) [18] and Co–7Al–7W (at.%) alloys [28]. The compositions of the studied alloys and our present alloy are summarized in the isothermal section of the Co–Al–W alloy in Fig. 1. In addition, the aging time spans discontinuously in all experiments, and the continuum precipitation kinetics and morphology evolution in medium supersaturation cobalt-based alloys have not yet been studied to cover early-stage precipitation to later-stage coarsening. The effect of aging temperature on

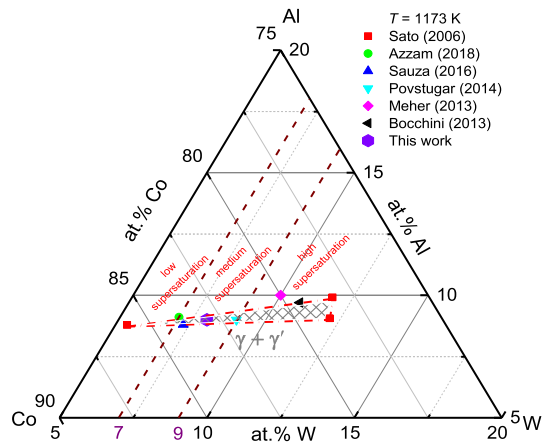


Figure 1 Composition region of Co–Al–W alloys in previous studies and present work at 1173 K.

continuous precipitation kinetics is still less studied, especially for the critical radius of the γ' phase and the PSD. Further research is significant for understanding the early-stage fast precipitation and evolution kinetics of the γ' phase in cobalt-based alloys with temperature change.

This research aims to investigate the precipitation kinetics of the γ' phase in a medium supersaturation Co–9Al–8W (at.%) alloy during 0.08 h, 0.5 h, 1 h, 2 h, 64 h, 136 h, 518 h, 808 h and 1000 h of aging at 1073 K and 1173 K. The evolution of the morphology, particle radius, particle number density, γ' phase volume fraction and microhardness of the alloy are extensively studied. The thermodynamic driving force for nucleation and the critical radius of the γ' phase, the interfacial energy, composition partitioning coefficients and interfacial compositional width between γ and γ' phases are clarified. Moreover, the evolution of the particle size distribution is discussed by comparing with the LSW [23, 24] theory, BW [25] and TIDC [26] models. The differences in the evolution of the γ' phase among low, medium and high supersaturation Co–Al–W alloys are discussed.

Experimental methods

Sample preparation

The Co–9Al–8W (at.%) alloy was produced by melting 99.95% pure Co, 99.99% pure Al and 99.97% pure W in a vacuum induction furnace a total of 4 times to obtain a uniform ingot with a mass of 30 g. The ingots were placed in a vacuum heat treatment

furnace for solution treatment at 1573 K for 24 h to ensure homogenization, after which the ingots were quenched in water.

Subsequently, these ingots were processed into cylinders with a diameter of 3 mm by electric spark wire cutting. To avoid severe oxidization of metal Co in a high-temperature environment, aging treatments were conducted in a vacuum tube furnace at 1073 K and 1173 K for 0.08 h, 0.5 h, 1 h, 2 h, 64 h, 136 h, 518 h, 808 h and 1000 h. The aged samples were then water quenched for further characterization.

Transmission electron microscopy and scanning electron microscopy

Energy-dispersive spectroscopy (EDS) in the scanning electron microscopy (SEM) was employed to measure the experimental sample before solution treatment. The composition of the sample obtained from a line scan involving 1024 counts under 20 kV was Co–9.2Al–7.8W (at.%), which is close to the nominal composition of the alloy.

The morphology of the γ' phase was observed by transmission electron microscopy (TEM) (FEI Tecnai G2 F20) at 200 kV and SEM (FEI Quanta 250F). After aging treatment, the samples were cut into thin slices with a thickness of ~ 0.5 mm by electric spark wire cutting and then mechanically polished to a thickness of ~ 50 μm . TEM foils were prepared by twin-jet electropolishing in an electrolyte of ethanol with 10% perchloric acid at 243 K and under 25–30 VDC. SEM samples were prepared by mounting the material in resin first and then polishing and chemically etching the material with an etching agent of hydrochloric acid and nitric acid in a 3:1 ratio at room temperature.

Atom probe tomography

To analyze the compositions of the γ and γ' phases and the spatial morphology of the γ' phases, samples that had been aged for 2 h at 1073 K and 1173 K were formed into rods with dimensions of $0.5 \times 0.5 \times 15$ mm^3 by two-stage microelectropolishing and analyzed by three-dimensional atom probe tomography (APT). An electrolyte containing 30 vol.% perchloric acid in acetic acid was used in the first stage at 15 VDC and room temperature, and for the second stage, electropolishing was carried out in a 5 vol.% perchloric acid in 2-butoxyethanol solution at 15 VDC. APT experiments were conducted by

using a local electrode atom probe (Cameca LEAP4000X Si) under an ultrahigh vacuum of 3×10^{-11} Torr at a specimen temperature of 40 K, a pulse frequency of 200 kHz, a laser pulse energy of 60 pJ and a target evaporation rate of 0.5%. The data reconstruction and quantitative analysis were performed with Cameca IVAS 3.6.8 software.

Microhardness measurement

Microhardness measurements of samples aged for 0 h, 2 h, 64 h, 136 h, 518 h, 808 h and 1000 h were performed with an HVS-1000Z Vickers microhardness tester. All measurements were performed at ambient temperature on samples that had been grounded and polished. The load of the hardness tester was 100 g, and the dwell time was 10 s. Each sample was tested 10 times, and the final hardness value was the average of the 10 readings.

Results

Effect of temperature on the morphology evolution of the γ' phases

The morphology evolution of the $L1_2$ long-range-ordered γ' - $\text{Co}_3(\text{Al}, \text{W})$ phase during aging at 1073 K and 1173 K was investigated via TEM and SEM. TEM micrographs of samples aged from 0.08 to 518 h are displayed in Figs. 2 and 3 shows SEM micrographs of samples aged for 808 h and 1000 h. Selected area electron diffraction (SAED) patterns along the [001] and [011] zone axes are shown in Fig. 2h and p, which confirm that the precipitates are γ' phases with a superlattice $L1_2$ structure.

It is conspicuous that aging temperature and time have a distinct influence on the precipitation process. Many γ' phases precipitate from the γ matrix after 0.08 h of aging at 1073 K and 1173 K, and these phases gradually grow and show distinct orientations along the [100] and [010] directions after 0.08 h of aging at 1173 K, as shown in Fig. 2i. However, at 1073 K, the obvious arrangement of the γ' phase is observed until 64 h in Fig. 2e. It is apparent that the γ' phase at 1173 K is of a larger size for the same aging time and displays a cuboidal shape earlier than that at 1073 K. The hardness difference between the soft γ matrix and the hard γ' phases makes the precipitates protrude from the matrix [29], as shown in Fig. 3c–d.

Aspect ratio and inter-precipitate distances of the γ' phases

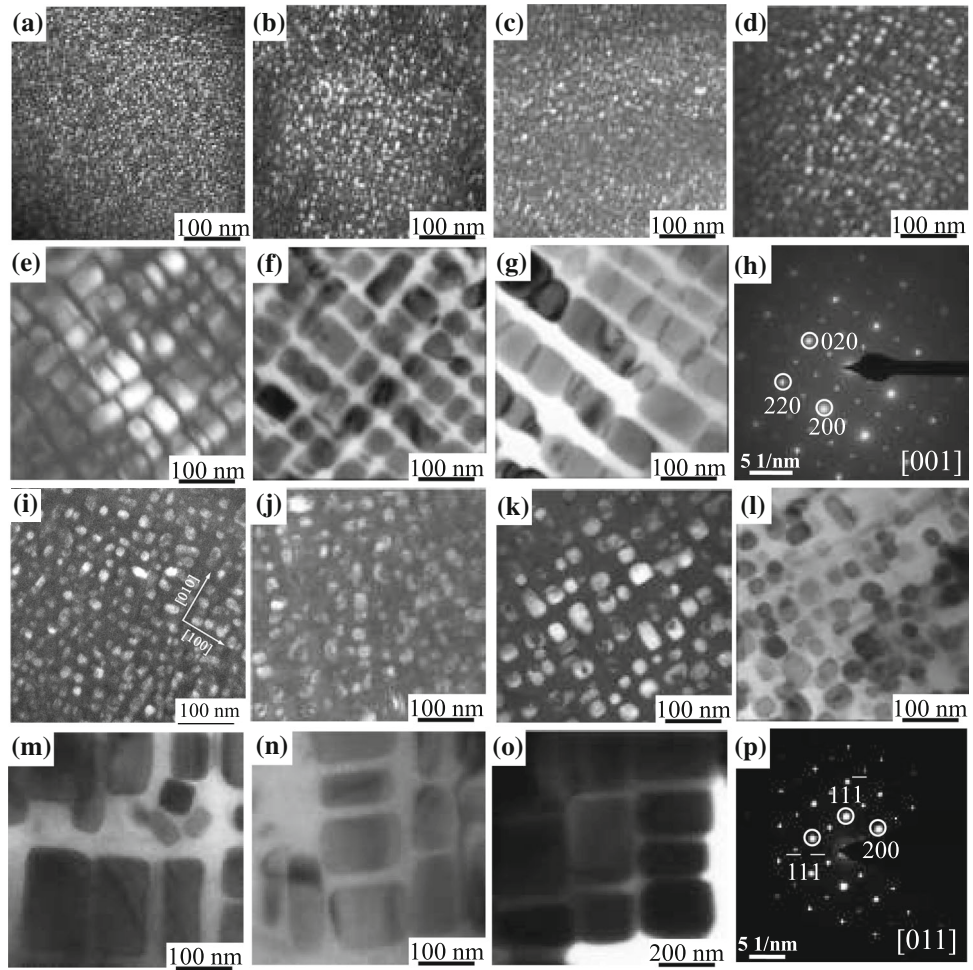
As shown in Fig. 2, as the aging time increased, the size of the γ' phase increased and the number of particles decreased. The shape evolution of the γ' phase was described by the aspect ratio of the long side to the short side of each γ' particle and the average aspect ratios (AARs) after 2 h of aging at 1073 K and 1173 K are listed in Table 1. The γ' phases connected by a concave neck were regarded as two particles. The sustained increase in the average aspect ratio indicated that the shape of the γ' phase gradually changed from an initial near-circular shape to a rectangular shape due to directional particle coarsening or merging of contiguous γ' phases. The larger values of AARs at 1173 K implied that high temperature promoted the coarsening of the γ' phase. The AAR values were very close after 2 h of aging at 1073 K and 1173 K, and the difference between the AARs of the two temperatures, as is characterized by ΔAAR , increased as the aging time increased. However, after 1000 h of aging, the ΔAAR decreased due to the enhanced coarsening connection of partial particles at 1073 K.

To characterize the particle interdistance, the average inter-precipitate distances (AIPDs) listed in Table 2 were measured by the average of the edge-to-edge distance from an individual particle to its nearest neighbor. The AIPDs increased continually during aging, wherein the values increased from 4.09 to 30.05 nm when aging at 1073 K and from 5.58 to 99.06 nm when aging at 1173 K. The large volume fraction of the γ' phase (see Fig. 8) made the AIPDs at 1073 K smaller than those at 1173 K, which led to a higher propensity for coalescence. In fact, under the influences of the γ/γ' interfacial energy and elastic strain energy, some γ' phases with rectangular shapes are present in Fig. 3b as a result of coarsening connections. However, the near cuboidal γ' phases were obvious at 1173 K, as shown in Fig. 3d.

Interface composition and element partition between the γ and γ' phases

Reconstructed three-dimensional atom maps of Co-9Al-8W (at.%) alloy aged for 2 h at 1073 K and 1173 K are shown in Fig. 4. The γ' phases were delineated by 9 at.% W isoconcentration surfaces, wherein the orange-colored areas represent the W-

Figure 2 TEM micrographs of Co–9Al–8W (at.%) alloy aged at 1073 K for **a** 0.08 h, **b** 0.5 h, **c** 1 h, **d** 2 h, **e** 64 h, **f** 136 h and **g** 518 h. TEM micrographs of Co–9Al–8W (at.%) alloy aged at 1173 K for **i** 0.08 h, **j** 0.5 h, **k** 1 h, **l** 2 h, **m** 64 h, **n** 136 h and **o** 518 h. SAED patterns along the **h** [001] zone axis after 2 h of aging at 1073 K and **p** [011] zone axis after 64 h of aging at 1173 K. Note that **d** is obtained with the (100) spot and corresponds to **h**. Moreover, note that **a–e**, **i**, **j** and **k** are dark-field micrographs, whereas the rest are bright-field micrographs.



rich γ' phase and the areas in blue correspond to the γ matrix. There were ~ 40 and ~ 30 million atoms in the reconstructed volumes at 1073 K and 1173 K, respectively, and the number of γ' particles covered was ~ 38 and ~ 6 , respectively. The average particle radius of the γ' phase was 5.87 nm at 1073 K and 17.51 nm at 1173 K. The γ' phases observed in thin slices were irregularly cuboidal in the sample aged for 2 h, which was in agreement with the TEM observations shown in Fig. 2d and l.

The proxigrams shown in Fig. 5 revealed the concentration profile across the γ/γ' phase interfaces. Evidently, there was a near constant distribution of concentration in the far field (2–4 nm away from the interface) after 2 h of aging. To show the partitioning behavior of alloy elements, the partitioning coefficient $K_i^{\gamma'/\gamma}$ ($i = \text{Co, Al, W}$), i.e., the ratio of each element concentration in the γ' and γ phases, was calculated by using the average concentration of the far field. The values were $K_{\text{Co}}^{\gamma'/\gamma} = 0.88$, $K_{\text{Al}}^{\gamma'/\gamma} = 1.09$ and

$K_{\text{W}}^{\gamma'/\gamma} = 3.47$ at 1073 K, whereas $K_{\text{Co}}^{\gamma'/\gamma} = 0.93$, $K_{\text{Al}}^{\gamma'/\gamma} = 1.01$ and $K_{\text{W}}^{\gamma'/\gamma} = 1.84$ at 1173 K. These coefficients indicate that Co partitions to the matrix while Al and W partition to the precipitate. The partitioning of W was more susceptible to temperature, which was confirmed by the obvious difference in $K_{\text{W}}^{\gamma'/\gamma}$.

The total concentrations of Al and W in the γ' phase were 22.83 at.% at 1173 K and 23.88 at.% at 1073 K, which approached the stoichiometric ratio of the $\text{Co}_3(\text{Al, W})$ phase. The slight difference from 3:1 indicated that a few Co atoms occupied the corner position of the L1_2 structure. The compositional width $\phi_{\gamma/\gamma'}$ of the γ/γ' interfaces of Co–9Al–8W (at.%) alloy was defined as the horizontal distance between the 10th and 90th percentiles of the composition difference height of W in the γ and γ' phases [30], so $\phi_{\gamma/\gamma'} = 2.61$ nm at 1073 K and $\phi_{\gamma/\gamma'} = 2.50$ nm at 1173 K. There were two main factors that affected the interface width characterized by APT: the

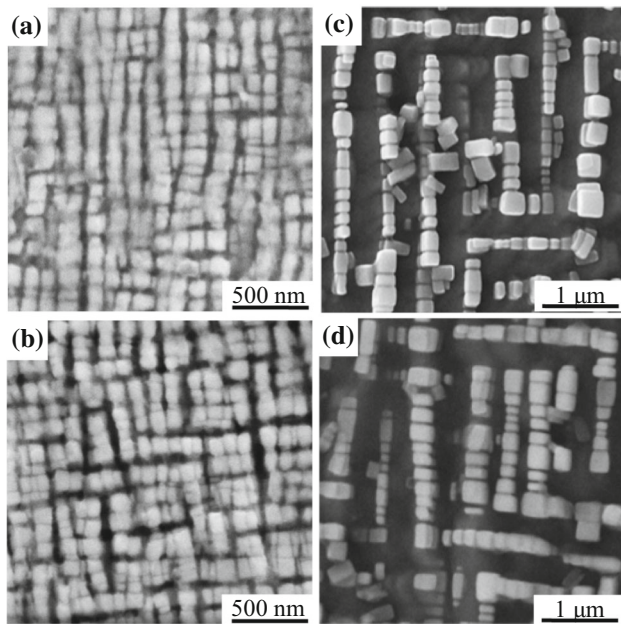


Figure 3 SEM micrographs of Co-9Al-8W (at.%) alloy aged at 1073 K for **a** 808 h and **b** 1000 h and at 1173 K for **c** 808 h and **d** 1000 h.

evaporation field strength of the element and the position of the interface. The univalent evaporation field strength of Al and W was 19 V/nm and 57 V/nm [31, 32], respectively, so the preferential evaporation of Al caused elongation of the interface width. In APT characterization, the resolution of the X or Y axis was lower than that of the Z axis. If the interface was parallel to the Z axis, the position of the side atoms will be disturbed, thereby widening the interface. Hence, the more perpendicular the interface was to the tip direction, the less likely it was that the interface width would be elongated.

Table 1 Average aspect ratios of the γ' phases in Co-9Al-8W (at.%) alloy aged at 1073 K and 1173 K

	2 h	64 h	136 h	518 h	808 h	1000 h
1073 K	1.22 ± 0.04	1.26 ± 0.04	1.32 ± 0.06	1.35 ± 0.04	1.40 ± 0.07	1.52 ± 0.11
1173 K	1.27 ± 0.05	1.42 ± 0.08	1.50 ± 0.07	1.57 ± 0.10	1.62 ± 0.05	1.65 ± 0.08
Δ AAR	0.05	0.16	0.18	0.22	0.22	0.13

Table 2 Average inter-precipitate distances of the γ' phases (nm) in Co-9Al-8W (at.%) alloy aged at 1073 K and 1173 K

	2 h	64 h	136 h	518 h	808 h	1000 h
1073 K	4.09 ± 0.21	5.88 ± 0.22	6.75 ± 0.40	12.66 ± 1.01	21.97 ± 0.89	30.05 ± 1.70
1173 K	5.58 ± 0.36	25.13 ± 3.66	26.96 ± 1.29	35.36 ± 2.38	94.56 ± 5.96	99.06 ± 7.97

Evolution kinetics and alloy hardness

The evolution kinetics of the γ' phases in the alloy can be roughly divided into three stages: nucleation, growth and coarsening. However, the precipitation kinetics of the γ' -Co₃(Al, W) phase in medium supersaturation cobalt-based superalloys have still not been studied with the effects of aging temperature. In this section, the evolutions of the average particle radius, particle number density, volume fraction, particle size distribution and alloy hardness at 1073 K and 1173 K are investigated quantitatively. The number of γ' particles for the statistics was greater than 200 for 1073 K and approximately 100 for 1173 K. For each aging temperature, the radius of each γ' particle was measured twice along the vertical and horizontal directions in the TEM and SEM micrographs, and the average of all measurements was taken as the average particle radius of the γ' phase $\langle r \rangle$ in Fig. 6a. The time exponents of $\langle r \rangle$ from 0.08 h to 1000 h were obtained by the linear fitting $\langle r_1 \rangle$ at 1073 K and $\langle r_2 \rangle$ at 1173 K, which revealed that $n_1 = 0.303 \pm 0.014$ and $n_2 = 0.313 \pm 0.005$. The slight deviation in the exponents from 1/3 was probably because there were many densely packed precipitates rather than a dilute solution, as described by the LSW theory [23, 24]. This phenomenon was supported by the results of Li et al. [33]. In addition, the average particle radii from the APT experiments for 2 h are marked with stars in Fig. 6, and these values are in accordance with the statistical results from the TEM micrographs.

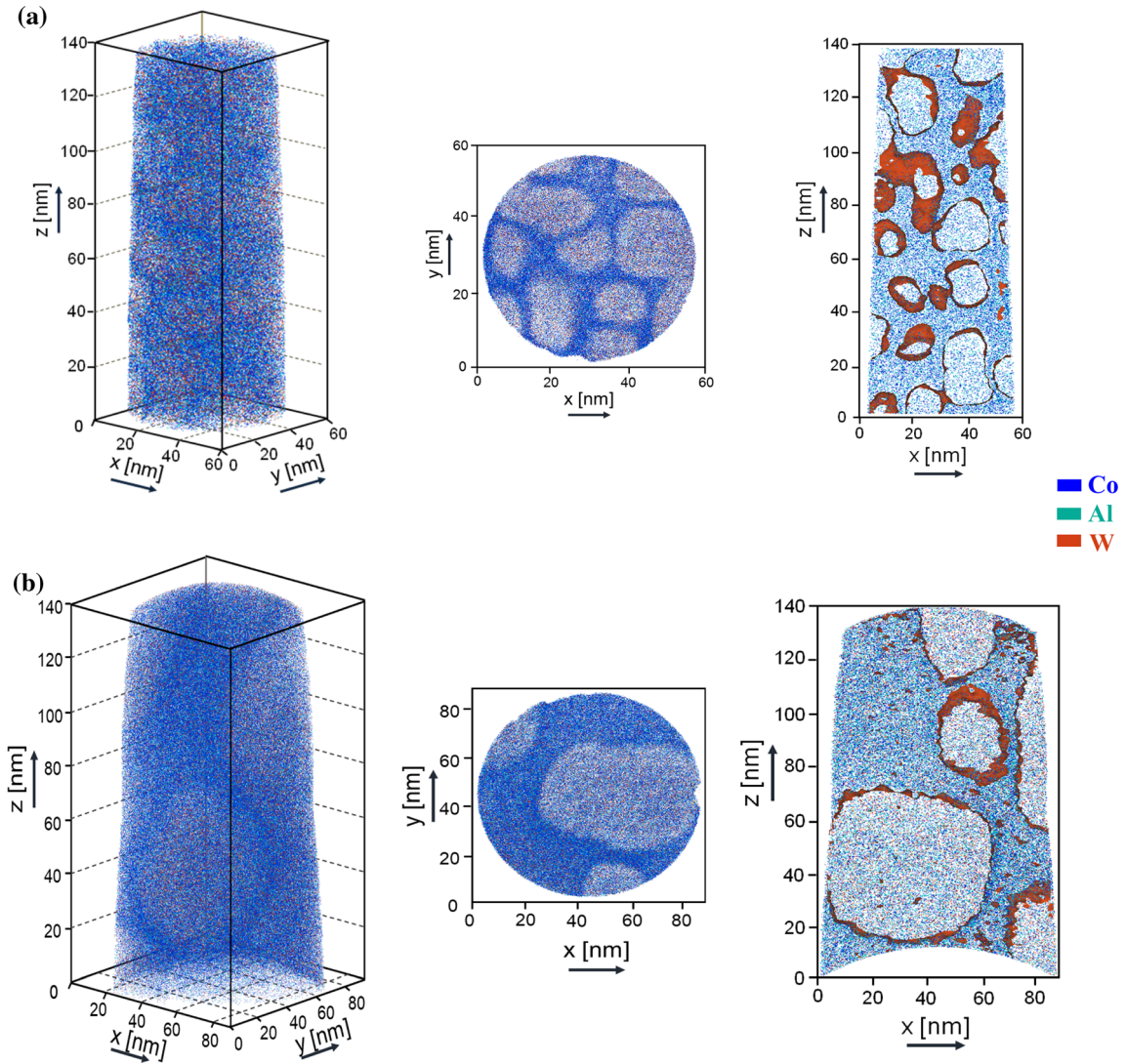
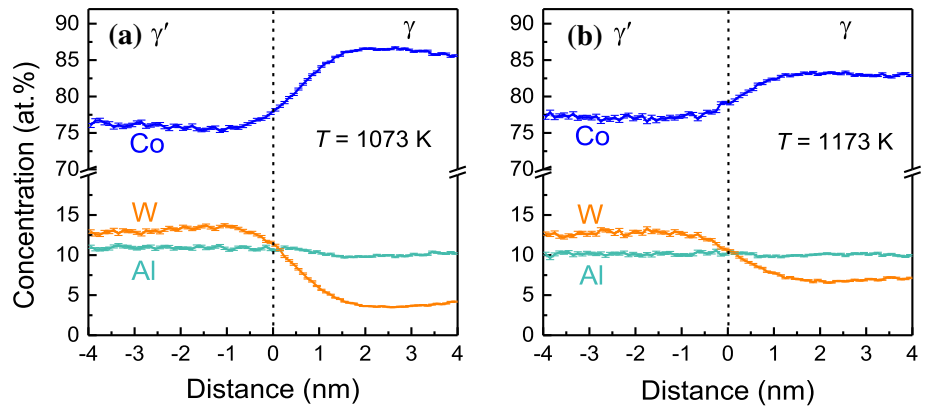


Figure 4 Reconstructed three-dimensional atom maps and two-dimensional slices (described by a 9 at.% W isoconcentration surface) of Co–9Al–8W (at.%) alloy aged for 2 h at **a** 1073 K and

b 1173 K, and the Co, Al and W atoms are represented by blue, green and orange, respectively.

Figure 5 Elemental concentration profiles of Co, Al and W across the γ/γ' interfaces of Co–9Al–8W (at.%) alloy aged for 2 h at **a** 1073 K and **b** 1173 K.



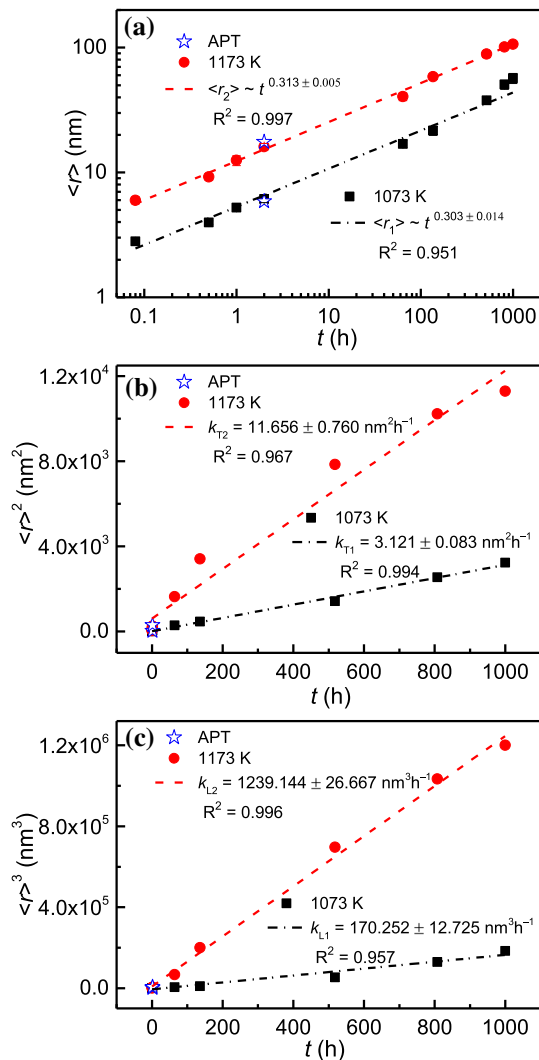


Figure 6 Evolution of the average particle radii **a** $\langle r \rangle$, **b** $\langle r \rangle^2$ and **c** $\langle r \rangle^3$ of the γ' phase in the Co-9Al-8W (at.%) alloy aged at 1073 K and 1173 K.

To identify the variation rate of the average particle radius $\langle r \rangle$ of the γ' phase, $\langle r \rangle^2$ and $\langle r \rangle^3$ are shown in Fig. 6b and c. The rate constants at 1073 K were $k_{T1} = 3.121 \pm 0.083 \text{ nm}^2\text{h}^{-1}$ and $k_{L1} = 170.252 \pm 12.725 \text{ nm}^3\text{h}^{-1}$, whereas they were $k_{T2} = 11.656 \pm 0.760 \text{ nm}^2\text{h}^{-1}$ and $k_{L2} = 1239.144 \pm 26.667 \text{ nm}^3\text{h}^{-1}$ at 1173 K. Hence, these rate constants increased by approximately fourfold and sevenfold, respectively, due to the accelerated diffusion when the aging temperature increased to 1173 K. The coefficients of determination indicated that the TIDC model had a better linear fitting at 1073 K, whereas the LSW theory fits well at 1173 K.

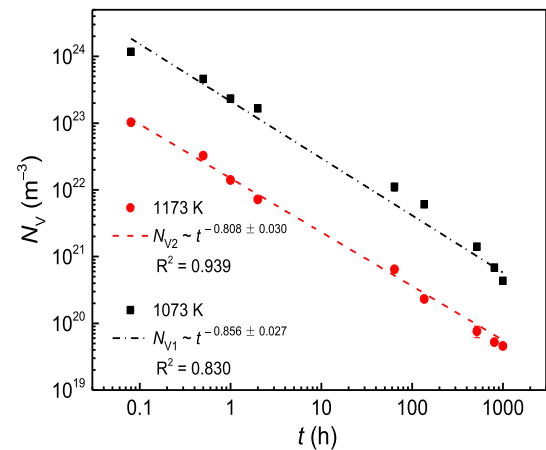


Figure 7 Evolution of the particle number density of the γ' phase in Co-9Al-8W (at.%) alloy aged at 1073 K and 1173 K.

Figure 7 shows the evolution of the particle number density of the γ' phase, wherein the increasing number density representing nucleation and the early growth stages are not observed even for a short 0.08 h aging time. The particle number density N_v , which describes the number of particles per unit volume, was calculated by $N_v = \frac{N_A}{2\langle r \rangle}$, where N_A is the number of γ' phase particles per unit area [34]. The time exponents for N_v were $n_{V1} = -0.856 \pm 0.027$ at 1073 K and $n_{V2} = -0.808 \pm 0.030$ at 1173 K, which were close to the value of -1 from the prediction of Kuehmann-Voorhees (KV) [35] in ternary alloy. In addition, the particle number density at 1073 K was larger than that at 1173 K because more nuclei formed.

It is generally known that a large volume fraction of the γ' phase can improve the creep resistance of

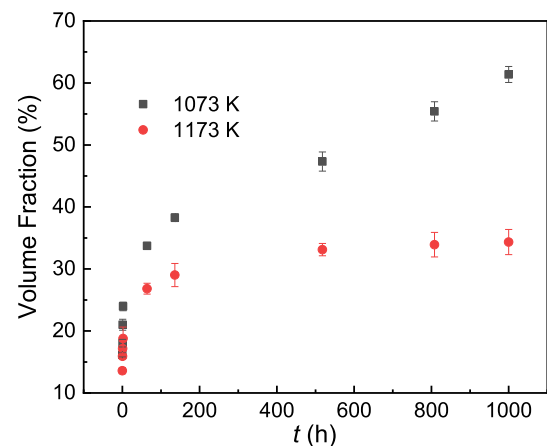


Figure 8 Variation in the volume fraction of the γ' phase in Co-9Al-8W (at.%) alloy aged at 1073 K and 1173 K.

superalloys [7, 8]. Figure 8 shows the variation in the volume fraction $V_{\gamma'}$ of the γ' phase, which increased rapidly when the aging time was less than 136 h, then increased to the maxima of $V_{\gamma'} = 61.37 \pm 1.29\%$ at 1073 K and $V_{\gamma'} = 34.34 \pm 2.03\%$ at 1173 K for an aging time of 1000 h. The volume fraction of the γ' phase after 0.08 h of aging at 1073 K reached $16.14 \pm 0.32\%$, and this large initial value affirmed the fast precipitation of γ' phases in cobalt-based superalloys.

As an important characterization for particle size homogeneity, the particle size distribution of the γ' phase is plotted in Fig. 9, in which the abscissa is the normalized equivalent radius $r/\langle r \rangle$ and the ordinate expresses the number of γ' phase particles for a given interval width (20% of $r/\langle r \rangle$) divided by the total γ' particle number and the scaled interval width [36]. This means that the region under each histogram was normalized to unity; consequently, the PSDs for different aging times can be compared directly. In these pictures, the histograms were experimental results at different aging times, the blue solid lines were the theoretical value from the LSW theory [23, 24], the green dash-dotted lines represent the results from the BW model [25], the red short-dashed lines represent the results from the TIDC model [26] and the black dashed lines represent the Gaussian fitting of the experimental values of PSD.

The peak values of the PSD decreased as the aging time increased, which was due to the inhomogeneity and dispersion of the particle size relying on the growth and coarsening of the γ' phase. For instance, due to Ostwald ripening, large particles grew continuously, and the small particles dissolved gradually. The peaks of the Gaussian fitted PSD were located at 1.0, and the width of the PSD increased with increasing aging time. The PSD became slightly wider as the aging temperature increased.

The evolution of the γ' phase directly affects the mechanical properties of the superalloy. As shown in Fig. 10, when t was less than ~ 136 h, the Vickers hardness increased fast during aging at variation rates of $m_1 = 0.570 \pm 0.058$ N/(mm²h) and $m_2 = 0.309 \pm 0.012$ N/(mm²h) for Co-9Al-8W (at.%) alloy aged at 1073 K and 1173 K, respectively. However, the variation rates of hardness after aging for 136 h were $m_3 = 0.046 \pm 0.008$ N/(mm²h) and $m_4 = 0.029 \pm 0.006$ N/(mm²h) at 1073 K and 1173 K, respectively, which were nearly 10 times lower than those at the early stage. This finding indicated that coarsened and connected γ' phases had limited contributions to hardness.

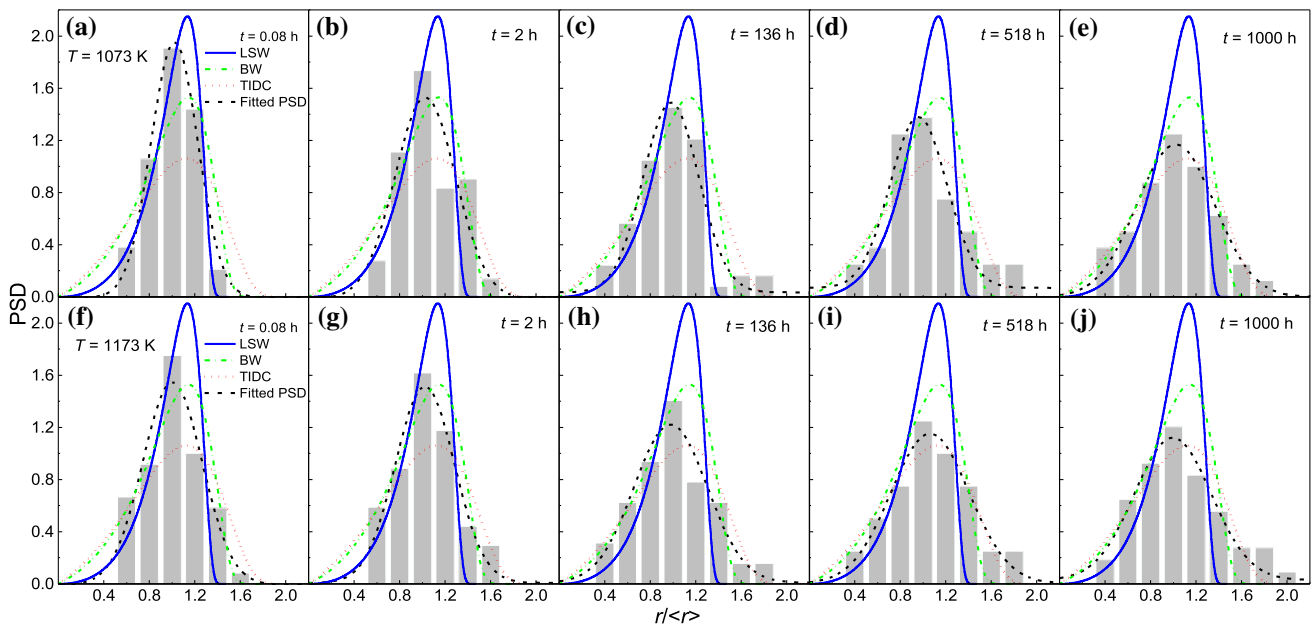


Figure 9 Variation in the particle size distribution of the γ' phase in Co-9Al-8W (at.%) alloy aged at 1073 K and 1173 K with respect to the aging time.

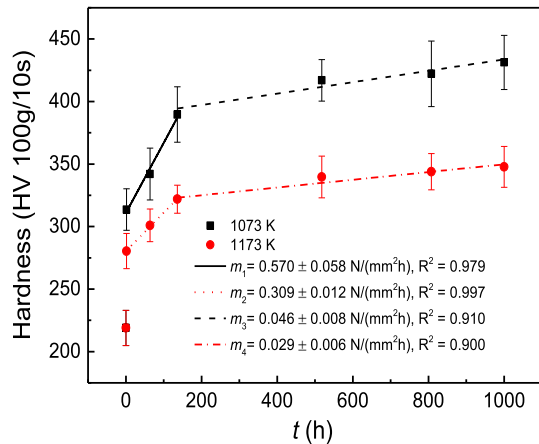


Figure 10 Variation in Vickers hardness for Co-9Al-8W (at.%) alloy aged at 1073 K and 1173 K.

Discussion

Fast precipitation and evolution of the γ' phases

In fact, the γ' phases already formed during water quenching after solution treatment but were difficult to detect due to their small size [18, 19]. This also explains why the nucleation stage was not observed in this work. It is remarkable that the increasing particle number density N_v disappeared in the Co-9Al-8W (at.%) alloy aged at 1073 K and 1173 K, which means that expeditious nucleation occurred earlier than 0.08 h of aging. Therefore, there was no distinct division among nucleation, growth and coarsening. The γ' phases entered the growth and coarsening stage quickly after a short aging time of 0.08 h, which conforms to the research results reported for Co-Al-W alloys [17–19, 28]. However, in nickel-based superalloys, the number density of the γ' phase increases to the maximum value after aging for 4 h at 873 K, and the incipient nucleation and growth stage is distinguished from the later growth and coarsening stage [37]. The difference in the initial precipitation rate between cobalt-based and nickel-based superalloys likely lies in the driving forces of the phase transformation and the radius of the critical nucleus, as discussed in “Nucleation regime” section.

When the γ' phases were stiffer than the matrix, they tend to become cuboidal as their sizes increase under the effect of the coherent strain energy between the γ and γ' phases [29]. The early γ' phases were small in size and spherical in shape at 1073 K and then evolved into cuboidal or rectangular shapes as

the aging time increased. In contrast, the γ' phases formed after 0.08 h of aging at 1173 K were larger in size and cuboidal in shape. Additionally, the arrangement of the γ' phases along the [100] and [010] directions was caused by the elastic inhomogeneity between the γ and γ' phases, which tended to minimize the elastic strain energy and caused the γ' phase to gradually become nearly cuboidal [38]. After long-term aging for 808 h and 1000 h, some γ' phases changed into rectangular shapes.

Coarsening mechanisms of the γ' phases

Regarding the kinetic stage of γ' phase precipitation, coarsening is usually distinguished by an exponential increase in the average particle radius, a decrease in the particle number density and a near constant volume fraction of the γ' phase in nickel-based alloys [37, 39]. In this Co-Al-W alloy, the variation in the volume fraction at 1073 K and 1173 K in Fig. 8 shows a large difference. After 136 h of aging, the volume fraction was nearly constant at 1173 K, indicating that steady-state coarsening was in progress, whereas the increasing volume fraction at 1073 K indicated that growth and coarsening occurred concomitantly. The decline in the particle number density in Fig. 7 verified that the precipitate kinetics of the Co-9Al-8W (at.%) alloy passed the nucleation-dominated stage.

The coefficients of determination R^2 of the average particle radius $\langle r \rangle$ in Fig. 6 indicated that $\langle r \rangle$ at 1173 K followed the $t^{1/3}$ of the LSW theory, as illustrated in Fig. 6a, which was also demonstrated by $\langle r \rangle^3$ vs. t in Fig. 6c. The average particle radius showed a better coefficient of determination R^2 for $\langle r \rangle^2$ vs. t at 1073 K.

As mentioned in “Fast precipitation and evolution of the γ' phases” section, the precipitation of the γ' phase in the cobalt-based alloy was so fast that it was still difficult to observe the initial nucleation stage [17–19]. Thus, the precipitation process of the γ' phase in the Co-Al-W alloy can be treated uniformly with growth and coarsening even during a short aging time of 0.08 h, which was consistent with the conclusion that all processes, including nucleation, growth and coarsening, do not occur in a strict sequence but overlap in time [40].

Precipitation kinetics and the concomitant alloy hardness

The differences in the rate constant of the average particle radius among high, medium and low supersaturation alloys at the same temperature were attributed to the concentration difference. For instance, the high W and Al contents facilitated the evolution of the γ' phase. This explained why the rate constant in the Co–10Al–10W (at.%) alloy [19] was larger than that in this medium supersaturation Co–9Al–8W (at.%) alloy. The rate constants in the growth stage and coarsening stage were quite different [41]. The longest aging time was 256 h for the Co–10Al–10W (at.%) alloy, where the growth was the dominant factor and produced a large rate constant. However, the aging time in our study was up to 1000 h, and the coarsening-dominated stage did have a lower rate constant.

As shown in Fig. 9, the peak values of the Gaussian fitted PSD were lower than those predicted by the LSW theory [23, 24], and the difference between the experimental value and the LSW theory prediction became greater when the volume fraction of the γ' phase increased with respect to aging time. However, the BW [25] and TIDC [26] models described the growth and coarsening of the γ' phase well for different precipitation stages: the early growth-dominated stage before 136 h of aging and the later concomitant growth and coarsening stages after 136 h of aging at 1073 K and 1173 K. The experimental PSD was close to the BW model in the early growth-dominated stage, and then the peaks were gradually lower than those of the BW model in the later concomitant growth and coarsening stages, especially for 1173 K. This shift occurred earlier. The fitted PSD was higher than that of the TIDC model before 136 h of aging, but they were in good agreement afterwards.

The volume fraction of 34.34% after 1000 h of aging was less than 58% in the Co–9Al–9W (at.%) alloy aged for 200 h at 1173 K [42], whereas it was greater than 31% in the Co–8.8Al–7.3W (at.%) alloy aged for 1024 h at 1173 K [17], indicating that W was favorable for the formation of the γ' phase. In addition, the volume fraction of the γ' phase at 1073 K was higher than that at 1173 K because the large undercooling degree at low temperature greatly promoted the precipitation of the γ' phases. As the most striking phenomenon, Vickers hardness changed

simultaneously with respect to the volume fractions of the γ' phase (see Figs. 8 and 10), which implied that the precipitation of the γ' phase increased the hardness of the Co–Al–W alloy, and the effect was more obvious in the early stage. A suitable combination of aging temperature and time can ensure the number and size of γ' phases to achieve good mechanical properties.

The increasing hardness of the alloy was mainly attributed to the precipitation of ordered intermetallics. In the early stage of aging ($t < \sim 136$ h), numerous small γ' phases distinctly hindered the movement of dislocations due to the coherent stress–strain field between the γ and γ' phases, thereby achieving precipitation strengthening. This phenomenon can be seen from the synchronous variation in the volume fraction of the γ' phase and the microhardness of the alloy, namely, a large volume fraction of γ' phases with a small particle size can lead to high alloy hardness [43], as shown by the results of 1073 K in Figs. 6a, 8 and 10. In the later stage of aging ($t > \sim 136$ h), the γ' phases grew and severely coarsened, and the hindrance of precipitates on dislocation movement was weakened. Hence, the large γ' phases weakened the strengthening effect, leading to a decrease in the rate of increase in the alloy hardness. The maximum alloy hardness was not reached, which was indicated by the absence of a plateau followed by a decrease in hardness. In addition, the hardness at 1073 K was higher than that at 1173 K, which was due to the numerous γ' phases with small size at 1073 K, and the dispersive strengthening effect was more conspicuous [44].

Nucleation regime

As displayed by the TEM micrographs, the γ' phases were greater in number and smaller in size at 1073 K than at 1173 K, which was due to the substantial undercooling degree $\Delta T = T - T_0$ at 1073 K, where T is the aging temperature and T_0 is the critical temperature for the precipitation of the γ' phase. The critical nucleation work ΔG^* required to form nuclei was inversely proportional to the square of the undercooling degree ΔT [45], $\Delta G^* = \frac{16\pi\phi^3 T_m^2}{3\Delta T^2 L_m^2}$, where ϕ is the free energy per unit area, L_m is the melting heat and T_m is the melting point. This equation suggests that the larger ΔT was the smaller the amount of work needed for the formation of the critical nucleus.

Thus, the nucleation work at 1073 K was smaller than that at 1173 K.

The critical nucleus was derived from the capillarity theory of classical nucleation, wherein the radius of the critical nucleus was generally calculated by $R^* = \frac{2\psi V_m}{(\Delta\bar{C})^T \mathbf{G}^\gamma \Delta\mathbf{C}^0}$. In this equation, ψ and V_m are the interfacial energy and molar volume of the γ' phase, respectively; \mathbf{G}^γ is the Hessian of the Gibbs energy of the γ phase; $\Delta\bar{C}$ is the equilibrium tie-line vector of the alloy, which is determined by the formula $\Delta\bar{C} = \bar{C}_W^\gamma - \bar{C}_W^\gamma$; and $\Delta\mathbf{C}^0 = \mathbf{C}_W^0 - \bar{C}_W^{\text{nominal}}$ represents the supersaturation vector. In addition, $\Delta G_m = (\Delta\bar{C})^T \mathbf{G}^\gamma \Delta\mathbf{C}^0$ represents the driving force for nucleation [46].

The growth or dissolution of the initial precipitates depends on the radius of the γ' nucleus being greater or less than the critical radius. The Hessian of the Gibbs energy \mathbf{G}^γ and the thermodynamic equilibrium compositions of γ and γ' phases, which were $\bar{C}_W^\gamma = 13.5$ at.% and $\bar{C}_W^\gamma = 2.25$ at.% at 1073 K and $\bar{C}_W^\gamma = 13.0$ at.%, $\bar{C}_W^\gamma = 4.25$ at.% at 1173 K, respectively, were calculated from the thermodynamic database of the Co–Al–W alloy [47]. Combined with the EDS measured composition of Co–9.2Al–7.8W (at.%), the driving forces for nucleation were $\Delta G_m = 264.24$ J mol⁻¹ and $\Delta G_m = 205.52$ J mol⁻¹ for 1073 K and 1173 K, respectively, which were greater than 190.4 J mol⁻¹ in Ni–Al alloy aged at 1103 K. The radius of the critical nucleus for the γ' phase was $R^* = 0.93$ nm at 1073 K and $R^* = 0.66$ nm at 1173 K in Co–9Al–8W (at.%) alloy (ψ and V_m come from “Interfacial energy of the γ/γ' phases” section), and these values were either approaching or slightly larger than the calculated values of 0.68 nm in Ni–12.5Al (at.%) alloy [36] and 0.75 nm in Ni–5.2Al–14.2Cr (at.%) alloy [37]. Such a small critical radius made the nucleus more resistant to dissolution in this alloy, and many nuclei evolved as γ' phases through solute diffusion. The fast precipitation of the γ' phase resulted in the absence of an increase stage in the particle number density after 0.08 h of aging, so the nucleation process was difficult to capture and needs further research by methods other than experiments, such as phase-field simulation. In fact, we have thoroughly investigated the early-stage evolution kinetics in a related work [41]. The nucleation stage reflected by increasing particle number density was

clarified, and three classical evolution stages were clearly divided in the work.

Interfacial energy of the γ/γ' phases

The morphology evolution of the γ' phase was controlled by free energy and followed the principle of energy minimization, so stable γ' phases were gradually formed when the free energy evolved to the minimum. The total free energy of the alloy system contained the chemical free energy, interfacial energy and elastic strain energy [38]. During the precipitation evolution of the γ' phase, these three component energies played a leading role in stages: the chemical free energy decreased after the nuclei formed, the interfacial energy first increased with the newly forming particles and then decreased with the coarsening of particles, and the elastic energy slowly increased as the particles precipitated, which resulted from the increasing volume fraction of precipitates.

The interfacial energy is related to the size of the γ' phase by following the Gibbs–Thomson theory $\langle r \rangle^3 - \langle r_0 \rangle^3 = k_L t$ with a rate constant $k_L = \frac{8\psi DC_e V_m}{9RT}$ [48, 49], where ψ is the interfacial energy between the precipitates and the matrix, C_e is the equilibrium concentration of solute atoms in the matrix, R is the gas constant (8.314 J mol⁻¹ K⁻¹), D is the diffusion coefficient of W in the matrix, $D = D_0 \exp(-\frac{Q}{RT})$, and Q is the diffusion activation energy. Calculating logarithms on both sides of $k_L T = A - \frac{Q}{RT}$, where $A = \ln(\frac{8\psi C_e V_m D_0}{9R})$. By linear fitting $\ln(k_L T)$ and T^{-1} (k_L and T come from Fig. 6c), A and $\frac{Q}{R}$ were abstracted from the intercept and the slope, wherein $A = 36.18$ and $Q = 215.12$ kJ mol⁻¹. Hence, the growth dynamics equation of the γ' phase in Co–9Al–8W (at.%) alloy can be expressed as $\langle r \rangle^3 - \langle r_0 \rangle^3 = 5.2 \times 10^{15} \cdot \frac{t}{T} \cdot \exp(-\frac{215.12}{RT})$. The calculated activation energy approached 223 kJ mol⁻¹ for the Co–8.8Al–7.3W (at.%) alloy obtained by Bocchini et al. [50]. $D_0 = 5.1 \times 10^{-6}$ m²s⁻¹ was the tracer diffusivity of W [51], so the diffusion coefficients of W were determined to be $D_1 = 1.72 \times 10^{-16}$ m² s⁻¹ at 1073 K and $D_2 = 1.34 \times 10^{-15}$ m² s⁻¹ at 1173 K. In addition, $V_m = 6.8 \times 10^{-6}$ m³ mol⁻¹ for Co₃(Al, W), and the C_e values from the thermodynamic calculations were 2.25 at.% and 4.25 at.% at 1073 K and 1173 K,

respectively. Accordingly, the interfacial energies of the γ/γ' phases were evaluated as $\psi_1 = 18 \text{ mJ m}^{-2}$ at 1073 K and $\psi_2 = 10 \text{ mJ m}^{-2}$ at 1173 K, which was consistent with 19 mJ m^{-2} and 10 mJ m^{-2} of Co–10Al–10W (at.%) alloy at the same temperature [19].

The γ' phases coarsened by means of coalescence or Ostwald ripening [52, 53], where the interfacial energy decreased simultaneously. In the coarsening stage, the elastic energy gradually dominated the morphology of the γ' phases due to the coherent strain between the γ and γ' phases. The anisotropy ratio was calculated by $\delta = 2C_{44}/(C_{11} - C_{12})$, where C_{ij} is the elastic modulus, and the values were $\delta_\gamma = 3.23$ for the γ phase and $\delta_{\gamma'} = 2.62$ for the γ' phase at 1173 K in the Co–Al–W alloy [54].

Conclusions

The morphology evolution, precipitation kinetics of the γ' -Co₃(Al, W) phase and the microhardness change in a medium supersaturation Co–9Al–8W (at.%) alloy aged at 1073 K and 1173 K were comprehensively investigated in this study. The morphology, average particle radius, particle number density, volume fraction and particle size distribution of the γ' phase were quantitatively explored from the early stage (0.08 h of aging) to the later coarsening stage (1000 h of aging), and the influences of the γ' phase morphology and volume fraction on the microhardness change in the alloy were clarified. Furthermore, the element partitioning behavior, driving force for nucleation, and interfacial energy of the γ/γ' phases were discussed. The following conclusions can be drawn from the results presented in this study:

1. The precipitation of the γ' phase was highly influenced by the aging temperature and time. At the same aging time, the particles were larger and displayed cuboidal shapes earlier at 1173 K than at 1073 K. The evolution kinetics from 0.08 h of aging to 1000 h of aging involved a process of growth and coarsening with decreasing particle number density and increasing volume fraction and alloy microhardness, especially before 136 h of aging.
2. Atom probe tomography showed the spatial morphology of the γ' phases and the composition proxigrams across the γ/γ' phase interfaces. The elemental concentrations within the γ matrix and γ' phase had a nearly constant distribution at 2 h of aging. The partitioning coefficients showed that W and Al partitioned to the γ' phase.
3. The time exponents of the average particle radius $\langle r \rangle$ at 1073 K and 1173 K were 0.303 and 0.313, respectively, which were close to the LSW theoretical value of 1/3. The rate constants of the γ' phase increased by approximately fourfold and sevenfold for the TIDC and LSW theories, respectively, when the aging temperature increased to 1173 K in the Co–9Al–8W (at.%) alloy.
4. The peak values of the Gaussian fitted PSD were lower than those predicted by LSW theory all the time; the PSD was close to the BW model in the early growth-dominated stage, whereas it matched well with the TIDC model in the later concomitant growth and coarsening stages. Moreover, the peak value of the PSD decreased with increasing aging, and the normalized equivalent radius $r/\langle r \rangle$ in accordance with the peak of the Gaussian fitted PSD was located at 1.0.
5. The driving forces for γ' phase nucleation were $264.24 \text{ J mol}^{-1}$ at 1073 K and $205.52 \text{ J mol}^{-1}$ at 1173 K, generating corresponding critical radii of 0.93 nm and 0.66 nm, which explains the expeditious precipitation within 0.08 h of aging. The diffusion activation energy for W in the γ matrix was identified as $215.12 \text{ kJ mol}^{-1}$ based on the rate constant, and the evaluated interfacial energies were 18 mJ m^{-2} at 1073 K and 10 mJ m^{-2} at 1173 K.

Acknowledgements

This work received financial support from the National Natural Science Foundation of China (No. 51571122) and the Fundamental Research Funds for the Central Universities (No. 30916015107).

Compliance with ethical standards

Conflict of interest The authors declare that there are no conflicts of interest.

References

- [1] Lee CS (1971) Precipitation-hardening characteristics of ternary cobalt-aluminum-X alloys. Ph.D. dissertation, University of Arizona
- [2] Sato J, Omori T, Oikawa K, Ohnuma I, Kainuma R, Ishida K (2006) Cobalt-base high-temperature alloys. *Science* 312:90–91
- [3] Yao Q, Xing H, Sun J (2006) Structural stability and elastics property of the $L1_2$ ordered $Co_3(Al, W)$ precipitate. *Appl Phys Lett* 89:97–131
- [4] Tsukamoto Y, Kobayashi S, Takasugi T (2010) The stability of γ' - $Co_3(Al, W)$ phase in Co–Al–W ternary system. *Mater Sci Forum* 654:448–451
- [5] Drapier JM, Coutouradis D (1968) Precipitation hardening of Co–Cr–Ta alloys. *Cobalt* 39:63–74
- [6] Viatour P, Drapier JM, Coutouradis D (1973) Stability of the γ' - Co_3Ti compound in simple and complex cobalt alloys. *Cobalt* 3:67–74
- [7] Titus MS, Suzuki A, Pollock TM (2012) Creep and directional coarsening in single crystals of new γ - γ' cobalt-base alloys. *Scripta Mater* 66:574–577
- [8] Tanaka K, Ooshima M, Tsuno N, Sato A, Inui H (2012) Creep deformation of single crystals of new Co–Al–W-based alloys with fcc/ $L1_2$ two-phase microstructures. *Philos Mag* 92:4011–4027
- [9] Suzuki A, Pollock TM (2008) High-temperature strength and deformation of γ/γ' two-phase Co–Al–W-base alloys. *Acta Mater* 56:1288–1297
- [10] Neumeier S, Freund LP, Göken M (2015) Novel wrought γ/γ' cobalt base superalloys with high strength and improved oxidation resistance. *Scripta Mater* 109:104–107
- [11] Bocchini PJ, Sudbrack CK, Noebe RD, Dunand DC, Seidman DN (2017) Microstructural and creep properties of boron- and zirconium-containing cobalt-based superalloys. *Mater Sci Eng A* 682:260–269
- [12] Wang D, Li YS, Shi SJ, Tong XW, Yan ZW (2020) Phase-field simulation of γ' precipitates rafting and creep property of Co-base superalloys. *Mater Des* 196:109077
- [13] Glazer J, Morris JW Jr (1988) The effect of the precipitate size distribution on the aging curve of order hardening alloys. *Acta Metall* 36:907–915
- [14] Mangen W, Nembach E (1989) The effect of grain size on the yield strength of the γ' -hardened superalloy NIMONIC PE16. *Acta Metall* 37:1451–1463
- [15] Fragomeni JM, Hillberry BM (1999) A micromechanical method for predicting the precipitation hardening response of particle strengthened alloys hardened by ordered precipitates. *Acta Mech* 138:185–210
- [16] Povstugar I, Zenk CH, Li R, Choi PP, Neumeier S, Dolotko O, Hoelzel M, Göken M, Raabe D (2016) Elemental partitioning, lattice misfit and creep behaviour of Cr containing γ' strengthened Co base superalloys. *Mater Sci Technol* 32:220–225
- [17] Souza DJ, Bocchini PJ, Dunand DC, Seidman DN (2016) Influence of ruthenium on microstructural evolution in a model Co–Al–W superalloy. *Acta Mater* 117:135–145
- [18] Azzam A, Philippe T, Hauet A, Danoix F, Locq D, Caron P, Blavette D (2018) Kinetics pathway of precipitation in model Co–Al–W superalloy. *Acta Mater* 145:377–387
- [19] Meher S, Nag S, Tiley J, Goel A, Banerjee R (2013) Coarsening kinetics of γ' precipitates in cobalt-base alloys. *Acta Mater* 61:4266–4276
- [20] Guan Y, Liu YC, Ma ZQ, Li HJ, Yu HY (2020) Precipitation and coarsening behavior of γ' phase in CoNi-base superalloy under different aging treatments. *Vacuum* 175:109247
- [21] Qu SS, Li YJ, Wang CP, Liu XJ, Qian K, Ruan JJ, Chen YC, Yang YS (2020) Coarsening behavior of γ' precipitates and compression deformation mechanism of a novel Co–V–Ta–Ti superalloy. *Mater Sci Eng A* 787:139455
- [22] Baler N, Pandey P, Palanisamy D, Makineni SK, Phanikumar G, Chattopadhyay K (2020) On the effect of W addition on microstructural evolution and γ' precipitate coarsening in a Co–30Ni–10Al–5Mo–2Ta–2Ti alloy. *Materialia* 10:100632
- [23] Lifshitz IM, Slyozov VV (1961) The kinetics of precipitation from supersaturated solid solutions. *J Phys Chem Solids* 19:35–50
- [24] Wagner C (1961) Theorie der alterung von niederschlägen durch umlösen (Ostwald-reifung). *Z Elektrochem* 65:581–591
- [25] Brailsford AD, Wynblatt P (1979) The dependence of ostwald ripening kinetics on particle volume fraction. *Acta Metall* 27:489–497
- [26] Ardell AJ, Ozolins V (2005) Trans-interface diffusion-controlled coarsening. *Nat Mater* 4:309–316
- [27] Meher S, Banerjee R (2014) Partitioning and site occupancy of Ta and Mo in Co-base γ/γ' alloys studied by atom probe tomography. *Intermetallics* 49:138–142
- [28] Vorontsov VA, Barnard JS, Rahman KM, Yan HY, Midgley PA, Dye D (2016) Coarsening behaviour and interfacial structure of γ' precipitates in Co–Al–W based superalloys. *Acta Mater* 120:14–23
- [29] Wagner R, Kampmann R, Voorhees PW (2001) Homogeneous second-phase precipitation. In: Kostorz G (ed) *Phase transformations in materials*. Wiley-VCH, New York, pp 309–407

- [30] Plotnikov EY, Mao ZG, Noebe RD, Seidman DN (2014) Temporal evolution of the $\gamma(\text{fcc})/\gamma'(\text{L1}_2)$ interfacial width in binary Ni–Al alloys. *Scripta Mater* 70:51–54
- [31] Tsong TT (1978) Field ion image formation. *Surf Sci* 70:211–233
- [32] Miller MK, Forbes RG (2014) *Atom-probe tomography: the local electrode atom probe*. Springer, New York
- [33] Li YZ, Puczak F, Oehring M, Wang L, Paul J, Lorenz U, Yao ZK (2017) Thermal stability of γ' phase in long-term aged Co–Al–W alloys. *J Alloys Compd* 729:266–276
- [34] Russ JC, Dehoff RT (2001) *Practical stereology*, 2nd edn. Plenum Press, New York
- [35] Kuehmann CJ, Voorhees PW (1996) Ostwald ripening in ternary alloys. *Metall Mater Trans A* 27:937–943
- [36] Plotnikov EY, Mao ZG, Baik SI, Yildirim M, Li YS, Cecchetti D, Noebe RD, Martin G, Seidman DN (2019) A correlative four-dimensional study of phase-separation at the subnanoscale to nanoscale of a Ni–Al alloy. *Acta Mater* 171:306–333
- [37] Sudbrack CK, Yoon KE, Noebe RD, Seidman DN (2006) Temporal evolution of the nanostructure and phase compositions in a model Ni–Al–Cr alloy. *Acta Mater* 54:3199–3210
- [38] Wang JC, Osawa M, Yokokawa T, Harada H, Enomoto M (2007) Modeling the microstructural evolution of Ni-base superalloys by phase field method combined with CAL-PHAD and CVM. *Comp Mater Sci* 39:871–879
- [39] Booth-Morrison C, Weninger J, Sudbrack CK, Mao ZG, Noebe RD, Seidman DN (2008) Effects of solute concentrations on kinetic pathways in Ni–Al–Cr alloys. *Acta Mater* 56:3422–3438
- [40] Ratke L, Voorhees PW (2002) Nucleation, growth and coarsening. In: *Growth and coarsening*. Engineering materials. Springer, Berlin, Heidelberg
- [41] Shi SJ, Yan ZW, Li YS, Muhammad S, Wang D, Chen S, Jin SS (2020) Phase-field simulation of early-stage kinetics evolution of γ' phase in medium supersaturation Co–Al–W alloy. *J Mater Sci Technol* 53:1–12. <https://doi.org/10.1016/j.jmst.2020.02.038>
- [42] Bauer A, Neumeier S, Pyczak F, Singer RF, Göken M (2012) Creep properties of different γ' -strengthened Co-base superalloys. *Mater Sci Eng A* 550:333–341
- [43] Bocchini PJ, Dunand DC (2018) Dislocation dynamics simulations of precipitation-strengthened Ni- and Co-based superalloys. *Materialia* 1:211–220
- [44] Goodfellow AJ, Galindo-Nava EI, Schwalbe C, Stone HJ (2019) The role of composition on the extent of individual strengthening mechanisms in polycrystalline Ni-based superalloys. *Mater Des* 173:107760
- [45] Abbaschian R, Abbaschian L, Reed-Hill RE (2009) *Physical metallurgy principles*, 4th edn. Cengage Learning, Stamford
- [46] Philippe T, Blavette D, Voorhees PW (2014) Critical nucleus composition in amulticomponent system. *J Chem Phys* 141:124306
- [47] Cui YF, Zhang X, Xu GL, Zhu WJ, Liu HS, Jin ZP (2011) Thermodynamic assessment of Co–Al–W system and solidification of Co-enriched ternary alloys. *J Mater Sci* 46:2611–2621. <https://doi.org/10.1007/s10853-010-5115-y>
- [48] Ardell AJ, Nicholson RB (1966) The coarsening of γ' in Ni–Al alloys. *J Phys Chem Solids* 27:1793–1794
- [49] Smallman RE (1985) *Modern physical metallurgy*, 4th edn. Butterworth, London
- [50] Bocchini PJ, Sudbrack CK, Noebe RD, Seidman DN (2018) Temporal evolution of a model Co–Al–W superalloy aged at 650 °C and 750 °C. *Acta Mater* 159:197–208
- [51] Naghavi SS, Hegde VI, Wolverson C (2017) Diffusion coefficients of transition metals in fcc cobalt. *Acta Mater* 132:467–478
- [52] Voorhees PW (1985) The theory of ostwald ripening. *J Stat Phys* 38:231–252
- [53] Calderon HA, Voorhees PW, Murray JL, Kostorz G (1994) Ostwald ripening in concentrated alloys. *Acta Metall Mater* 42:991–1000
- [54] Jokisaari AM, Naghavi SS, Wolverson C, Voorhees PW, Heinonen OG (2017) Predicting the morphologies of γ' precipitates in cobalt-based superalloys. *Acta Mater* 141:273–284

Publisher's Note Springer Nature remains neutral with regard to jurisdictional claims in published maps and institutional affiliations.